Ocean Engineering 266 (2022) 112750

Contents lists available at ScienceDirect

Ocean Engineering

journal homepage: www.elsevier.com/locate/oceaneng

Identification of the safety operating envelope of a novel subsea shuttle tanker

Yucong Ma *, Yihan Xing

Department of Mechanical and Structural Engineering and Material Science, University of Stavanger, 4036, Stavanger, Norway

ARTICLE INFO

Keywords:
Safety operating envelope
Submarine manoeuvring
Subsea shuttle tanker
Emergency recovery action
Flooding
Hydroplane jam

ABSTRACT

A baseline Subsea Shuttle Tanker (SST) was proposed as a cost-efficient maritime transportation method. It is designed to be a 164 m length, 17 m beam autonomous underwater vessel with a cargo capacity of over 16,000 m^3. One of the crucial topics for such underwater vehicles is recoverability during undesired malfunctions. A Safety Operating Envelope (SOE) must be identified for military submarines. It considers the submersibles' malfunctions, including partial flooding, jam-to-rise, and jam-to-dive. This paper aims to identify the SOE to enclose the safety operation zones of the SST. In this work, a planar SST manoeuvring simulation model considering the combined contributions from hydrodynamic loads, compensation tank blowing, propeller thrust, and control planes is derived based on semi-empirical formulas. Second, standard operating procedures of recovery actions are established to cope with each malfunction. After that, free-running simulations are conducted. Three cases are presented to discuss SST recovery responses during each incident. Finally, the SOE of the SST is identified. This established SOE determines the SST's feasible speed and depth excursion ranges from an operational safety perspective. The safety depth is sufficient for the SST to recover from a jam-to-rise failure. Moreover, the study found that the existing safety factor on the structural design suggested by the Norwegian classification society Det Norske Veritas (DNV) naval submarine code is exceedingly conservative and potentially leads to a heavy and complex SST structure. The SOE helps reduce the designed collapse depth from the operational safety perspective and contributes to reduced material cost and considerable payload capacity. Also, this work fills in the blanks of SOE analysis on commercial submersibles.

1. Introduction

1.1. Subsea shuttle tanker

In a subsea hydrocarbon production operation, pipelines are commonly used to transport fluids between wells, floating production units, and onshore facilities. However, installing submarine pipelines can be expensive for trunk lines and marginal fields, as this cost grows excessively with the increase in transportation distance. Besides, pipeline maintenance and repair are time-consuming and require a full-line or partial shutdown, which is also economically undesirable. The tanker ship is a more flexible and economically feasible option for trunk lines. It can be deployed quickly to new fields to cope with unpredictable situations like a sudden increased need. However, the operation of shuttle tankers is highly weather dependent. During loading and offloading, a nonideal environmental condition may cause severe relative motion between a tanker ship and the floating production unit. This may further cause delay or the risk of collision. Therefore, a subsea tanker concept was proposed as a potential alternative for the above-mentioned transportation methods. The subsea shuttle tanker can reduce the field installation cost by eliminating some floating loading systems and risers. This contributes to developing subsea production units, considered the "factories of the future" in the offshore oil & gas industry and extensively developed for arctic regions and deep water (Schjølberg and Utne, 2015).

The idea of utilising large freight submarines for hydrocarbon transportation is not new. In 1971, Jacobsen demonstrated technical and economic evaluation of using submersibles between 20,000 and 42,000 DWT to transport crude oil between Alaska/North Canada and Tromsø (Jacobsen, 1971). Later in the seventies and eighties, several submarine tanker concepts were proposed to transport crude oil or liquified natural gas (Jacobsen et al., 1983; Jacobsen and Murphy, 1983; Moloney, 1974; Taylor and Montgomery, 1977). These submersibles were typically designed to sail at 13–20 knots speed and use nuclear or

* Corresponding author.
E-mail address: yucong.ma@uis.no (Y. Ma).

https://doi.org/10.1016/j.oceaneng.2022.112750
Received 21 March 2022; Received in revised form 25 September 2022; Accepted 26 September 2022
Available online 6 October 2022
0029-8018/© 2022 The Author(s). Published by Elsevier Ltd. This is an open access article under the CC BY license (http://creativecommons.org/licenses/by/4.0/).

diesel engines as the power source. Due to technical constraints, studies of freight submarines were halted from the 1990s until recent times. In 2019 and 2020, Equinor Energy AS brought up a subsea shuttle system concept in two research disclosures (Ellingsen et al., 2020; Equinor Energy AS, 2019), which demonstrated the application of large submarine drones for transportation between ports, offshore platforms, and subsea wells. It can carry various cargos, such as hydrocarbon, CO_2, electric power, equipment, and other chemicals. Later, Xing (Xing et al., 2021a) discussed critical design considerations related to this concept and limited the scope of the subsea shuttle system to liquid CO_2 transportation. Based on works conducted by Equinor and Xing, a 33, 619-tonne baseline Subsea Shuttle Tanker (SST) was proposed (as illustrated in Fig. 1) (Ma et al., 2021b). It is feasible for marginal fields compared to existing and subsea pipelines (Ma et al., 2021a; Xing et al., 2021b). The SST's preliminary design parameters used in this study are listed in Table 1.

1.2. Safety operating envelope

SST accidents may cause loss of the vessel, leakage of CO_2, leakage of hydrocarbon, and damage to offshore facilities or third parties. These consequences can further lead to property loss, environmental pollution, or casualties. Therefore, safety during operation looms large in the design of the SST. The concept that brings safety and dynamics of control of SST together is the Safety Operating Envelope (SOE). The SOE is a set of manoeuvring limits that outlines the safe operating zone of the system. As manoeuvring limits vary with the system, the appearance of the SOE is also different. It is straightforward to use the SOE to determine the operational safety of systems, and the SOE has been used on a wide variety of vessels such as ships (Kery et al., 2018), submarines, and aeroplanes (Lombaerts et al., 2013).

The SOE for the SST is adapted from the existing experiences on naval submarines, where its application has been practised for decades and is required by the state-of-the-art standard the Norwegian classification society Det Norske Veritas (DNV) naval submarine code (DNV, 2018). It presents manoeuvring limits on the submarine operation to guarantee its survivability if a credible failure happens. Marchant and Kimber (2014) discussed that an SOE could be depicted in two ways. One is the manoeuvring limitation diagrams, which present the safety limits on the control plane pitch angle. The other is the safe manoeuvring envelopes, which present the safety limits on the initial trim conditions. In this work, the safe manoeuvring envelope is presented.

The application of SOE on submarines is not new and necessary. Early in 1966, Giddings and Louis studied the emergency recovery of a 150-tonne submarine under surface jams and flooding (Giddings and Louis, 1966). In 1968, the INS Dakar submarine from the Israeli navy encountered an aft plane jam and exceeded collapse depth with 69 casualties (Tingle, 2009). Burcher and Rydill (1994) discussed the impact of SOE on submarine design and concluded that it significantly affects the submarine dynamics and control systems. This is confirmed by British defence technology company QinetiQ, which studied the effect of aft control plane setup and found that an X aft configuration is the most blessing design (QinetiQ, 2018). Park and Kim (2017, 2018) investigated submarine depth excursion and designed an SOE protection system during an aft control plane jam.

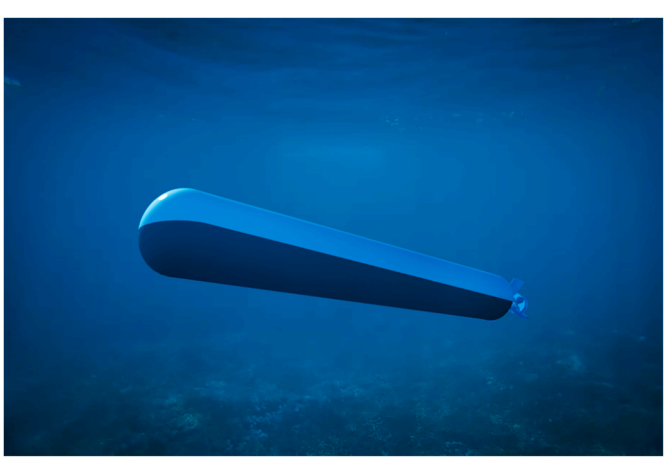

Fig. 1. Subsea Shuttle Tanker illustration.

Table 1
SST Main Design Parameters summarised from (Ma et al., 2021b).

Parameter description	Value	Unit
Length (l_{sst})	164	m
Beam (d_{sst})	17	m
Mass displacement (m_{sst})	3.36×10^4	tonne
Pitch moment of inertia (I_{yy})	7.60×10^{10}	kg•m^2
Centre of gravity ($[x_g, y_g, z_g]$)	[0, 0, 5.78]	m
Safety diving depth	40	m
Nominal diving depth	70	m
Collapse diving depth	190	m

As exemplified in Fig. 2, a typical submarine SOE is a depth versus velocity diagram. It represents the submarine's survivability when encountering credible failures, such as flooding and control plane jams. In this way, the SOE minimises the vessel's operational risk by ensuring adequate manoeuvrability under pre-identified failures. The safety operating envelop of the SST can be divided into six zones:

- Jam-to-rise avoid zone: the SST risks breaching the surface when a control plane jam happens.
- Restricted operation zone: the SST is less manoeuvrable when sailing at a higher speed. The maximum pitch angle and maximum control plane angle must be restricted.
- Unrestricted operation zone: the SST is free to operate without limitation when its depth and velocity locate in this zone.
- Flood avoid zone: SST control planes cannot generate enough lift force at slow speed when free-flooding compartments are filled with water. Therefore, the SST may sink and exceed the collapse diving depth.

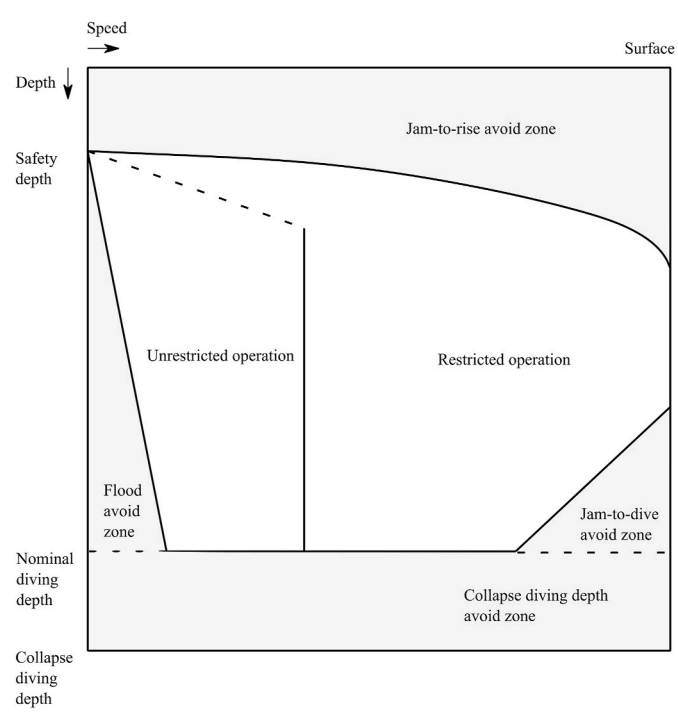

Fig. 2. Safety operating envelope example.

- Jam-to-dive avoid zone: the SST has the risk of exceeding the collapse diving depth when a control plane jam happens.
- Collapse diving depth avoid zone: the SST sails above its nominal diving depth.

The detailed considerations of the provided incidents are provided in Section 3. Even though an SOE analysis is most frequently performed on in-service submarines as mitigation against loss-of-vessel during incidents, it is also adapted into the design process for new submarines. The SOE can influence the design parameters, such as speed and depth. Also, it can highlight any potential problems with hydrodynamics or control systems design at the final design stage.

SOE analysis can help the SST determine its service speed and operating depth. The SOE examines the SST service speed feasibility from an emergency recovery perspective. For instance, the baseline SST is designed to travel at a 6-knot slow speed with 90% lower energy consumption than a tanker ship (Ma et al., 2021b). However, Fig. 2 indicates that such a slow speed may make the SST unrecoverable during flooding. Because of this, a minimum service speed needs to be imposed during SST operation. In addition, the SOE can reduce the safety factor applied to the structural design and allow the SST to increase its operating depth. For the baseline SST whose nominal diving pressure is 7 bar (70 m, ref. Section 3), A safety factor of 2.7 is required per DNV naval submarine code (DNV, 2018). This gives an exceedingly high collapse depth of 190 m, i.e., a 19-bar design pressure, which leads to heavy and complex steel construction. Nevertheless, the collapse diving depth can be reduced by understanding SST recovery behaviour under a malfunction. Therefore, a smaller safety factor is proposed from the operational safety point of view. As a side note, the depth and seabed properties does not affect the SOE. In contrast, the SOE helps the decision makers to decide the depth and seabed clearance of an SST operation.

In contrast to naval submarines, where SOE analysis has been performed for decades, the published implementations of such analyses on commercial submersibles are still blank. Also, as a novel merchant vessel, the SST differs from conventional submarines in several ways. For instance, the hazards and consequences differ as the SST travels much slower than a naval submarine. In addition, compared to a naval submarine whose structures and machinery take up approximately 80% dry weight, the SST has to have a minimum 50% payload of its dry weight to be economically attractive (Xing et al., 2021a). Thus, the collapse pressure of the SST is much lower than a naval submarine to avoid a heavy pressure hull. These differences will make the identified SST SOE very different from the SOE for a naval submarine. Therefore, this paper also helps to contribute knowledge on SOE analysis for commercial and non-military submersibles. The methodology presented in this paper can be applied to other novel subsea vessels under development aiming to contribute to a low-carbon maritime sector, such as civilian submersibles and freight gliders (Xing, 2021).

1.3. Structure of paper

This paper presents the generation of the SST safety operating envelope. Section 2 introduces the setup of SST manoeuvring model. Section 3 describes the malfunctions and the corresponding Standard Operating Procedure (SOP) during recovery. Finally, the SOE is generated in Section 4 and the findings are summarised in Section 5.

2. Manoeuvring simulation model

The setup of the SST manoeuvring model is described in this section. The model is developed in MATLAB Simulink 2021a environment, which is a block-diagram-based graphical programming environment (MathWorks, 2022). It is utilised to build up a physical multibody system in a graphical-based manner and has been extensively used in the area of subsea drones. The manoeuvring model is general and can be facilitated with different functions to solve various problems, such as depth control (Ma et al., 2020) and hovering (Ma et al., 2022). A decoupled 3 degrees of freedom (DoF) planar model is proposed in this work instead of a fully coupled 6 DoF model, as used in Park and Kim (Park and Kim, 2017, 2018). This is enough to represent the emergency recovery action. Ross (Ross et al., 2004) found that a submersible can be divided into two non-interacting subsystems: longitudinal and lateral. This is especially applicable to a port-starboard symmetric slender body like a submarine (Tinker, 1982). The coordinate system contains a North-East-Down (NED) coordinate system with its origin fixed to the Earth's reference point and a body-fixed reference frame located at the SST centre of buoyancy (CoB). The coordinate system used in this study is presented in Fig. 3.

2.1. Plant model

Longitudinal subsystem equations of motion considering surge, heave, and pitch written in a vectorial format using Fossen notation (Fossen, 2011) are presented in (1) and (2):

$$\dot{\boldsymbol{\eta}} = \boldsymbol{J}_{\boldsymbol{\Theta}}(\boldsymbol{\eta})\boldsymbol{\nu} \tag{1}$$

$$\boldsymbol{M}\dot{\boldsymbol{\nu}} + \boldsymbol{C}(\boldsymbol{\nu})\boldsymbol{\nu} + \boldsymbol{D}(\boldsymbol{\nu})\boldsymbol{\nu} + \boldsymbol{g}(\boldsymbol{\eta}) = \boldsymbol{\tau} \tag{2}$$

where $\boldsymbol{\eta}$ is a vector consisting of NED position and Euler angles, $\boldsymbol{\nu}$ is the linear and angular velocity in the body-fixed system, $\boldsymbol{J}_{\boldsymbol{\Theta}}(\boldsymbol{\eta})$ is the Euler transformation matrix, $\boldsymbol{M}$ is the system mass matrix consisting of SST mass and added mass, $\boldsymbol{C}(\boldsymbol{\nu})$ is the Coriolis-centripetal matrix, $\boldsymbol{D}(\boldsymbol{\nu})$ is the damping matrix, $\boldsymbol{g}(\boldsymbol{\eta})$ is the force vector considering gravitational and buoyancy forces, $\boldsymbol{\tau}$ is the control force vector.

Expand the kinematic equation (1) into the component form using Euler angle representation as:

$$\underbrace{\begin{bmatrix} \dot{N} \\ \dot{D} \\ \dot{\theta} \end{bmatrix}}_{\dot{\boldsymbol{\eta}}} = \underbrace{\begin{bmatrix} \cos\theta & \sin\theta & 0 \\ -\sin\theta & \cos\theta & 0 \\ 0 & 0 & 1 \end{bmatrix}}_{\boldsymbol{J}_{\boldsymbol{\Theta}}(\boldsymbol{\eta})} \underbrace{\begin{bmatrix} u \\ w \\ q \end{bmatrix}}_{\boldsymbol{\nu}} \tag{3}$$

In the dynamic equations of motion, the mass matrix $\boldsymbol{M}$ is presented as (4), the Coriolis-centripetal matrix is expressed as (5), and the damping matrix is written as (6).

$$\boldsymbol{M} = \begin{bmatrix} m - X_{\dot{u}} & 0 & mz_g \\ 0 & m - Z_{\dot{w}} & -Z_{\dot{q}} \\ mz_g & M_{\dot{w}} & I_{yy} - M_{\dot{q}} \end{bmatrix} \tag{4}$$

$$\boldsymbol{C}(\boldsymbol{\nu}) = \begin{bmatrix} 0 & 0 & 0 \\ 0 & m - Z_{\dot{w}} & -(m - X_{\dot{u}})u \\ 0 & (Z_{\dot{w}} - X_{\dot{u}}) & 0 \end{bmatrix} \tag{5}$$

$$\boldsymbol{D}(\boldsymbol{\nu}) = \begin{bmatrix} X_{|u|u}|u| & X_{wq}q & X_{qq}q \\ Z_{uq}q & Z_{|w|w} + Z_{uw}u & Z_{q|q|} \\ M_{uw}w & M_{|w|w} & M_{uq}u + M_{|q|q} \end{bmatrix} \tag{6}$$

where m is SST mass and z_g is the location of the vertical centre of

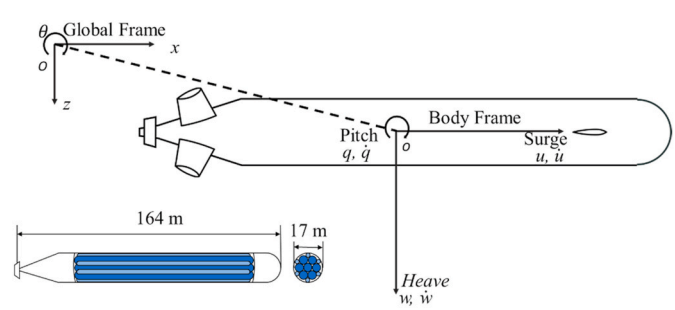

Fig. 3. SST coordinate system.

gravity. These are listed in Table 1. The applied hydrodynamic coefficients are listed in Table 2 and estimated as (7)–(25) following Prestero's study on REMUS AUV (Prestero, 2001).

The axial added mass $X_{\dot{u}}$ of the SST is calculated by the empirical formula provided by Blevins (1979), which estimates the added mass of an ellipsoid.

$$X_{\dot{u}} = -\frac{4\alpha\pi\rho}{3}\left(\frac{l_{sst}}{2}\right)\left(\frac{d_{sst}}{2}\right)^2 \tag{7}$$

where $\alpha = 0.021$ is an empirical parameter, l_{sst} is the SST length, and d_{sst} is the SST's beam.

The added mass of a circular slice submerged in water can be found in Faltinsen (1993):

$$m_a(x) = \pi\rho R(x)^2 \tag{8}$$

where $R(x)$ is the cross-section radius.

The crossflow added mass terms related to heave and pitch are calculated by integrating the added mass of circular slices along the body. These are expressed in (9)-(12):

$$Z_{\dot{w}} = -\int_{x_{tail}}^{x_{bow}} m_a(x)dx \tag{9}$$

$$M_{\dot{w}} = \int_{x_{tail}}^{x_{bow}} x m_a(x)dx \tag{10}$$

$$Z_{\dot{q}} = M_{\dot{w}} \tag{11}$$

$$M_{\dot{q}} = -\int_{x_{tail}}^{x_{bow}} x^2 m_a(x)dx \tag{12}$$

where $x_{bow} = 88.7$ m and $x_{tail} - 75.3$ m are positions of the bow and tail end, respectively.

The quadratic axial drag derivative can be estimated as:

$$X_{|u|u} = -0.5\rho c_d A_f \tag{13}$$

where $c_d = 0.145$ is the axial drag coefficient, $A_f = 227.0$ m^2 is SST frontal projected area.

The crossflow damping terms are expressed as:

$$Z_{|w|w} = -0.5\rho c_{dc}\int_{x_{tail}}^{x_{bow}} 2R(x)dx \tag{14}$$

$$M_{|w|w} = 0.5\rho c_{dc}\int_{x_{tail}}^{x_{bow}} 2xR(x)dx \tag{15}$$

$$Z_{|q|q} = 0.5\rho c_{dc}\int_{x_{tail}}^{x_{bow}} 2x|x|R(x)dx \tag{16}$$

$$M_{|q|q} = -0.5\rho c_{dc}\int_{x_{tail}}^{x_{bow}} 2x^3 R(x)dx \tag{17}$$

where c_{dc} is the crossflow drag coefficient of a cylinder. $c_{dc} = 1.1$ suggested by Hoerner (1965) is used.

Cross-term hydrodynamic derivatives are obtained as follows:

$$X_{wq} = Z_{\dot{w}} \tag{18}$$

$$X_{qq} = Z_{\dot{q}} \tag{19}$$

$$Z_{uq} = -X_{\dot{u}} \tag{20}$$

$$M_{uq} = -Z_{\dot{q}} \tag{21}$$

$$M_{uw_a} = -(Z_{\dot{w}} - X_{\dot{u}}) \tag{22}$$

SST body lift and lift-induced pitch moment are presented as (23) and (24), respectively.

$$Z_{uw} = -0.5\rho d^2 c_{yd\beta} \tag{23}$$

$$M_{uw_l} = -0.5\rho d^2 c_{yd\beta} x_{cp} \tag{24}$$

where $c_{yd\beta} = 0.003$ is the lift slope coefficient (Ref. Prestero (2001)) and $x_{cp} = -31.6$ m is the viscous force centre (Ref. Hoerner (1965)).

Finally, the total cross-term pitch moment hydrodynamic derivative is expressed as a summation of added mass contribution and body lift contribution:

$$M_{uw} = M_{uw_a} + M_{uw_l} \tag{25}$$

2.2. Compensation tanks blowing

The SST equips two compensation tanks located at the bow and aft free flooding compartments, as illustrated in Fig. 4. These tanks are filled with ballast during regular operation. The ballast volumes inside compensation tanks are depended on the cargo tank condition to ensure neutral buoyancy, i.e., the weight of the SST is equal to buoyancy. During the emergency rising manoeuvre, the compensation tank blowing is performed. The tank blowing of the SST follows the same process with a crewed naval submarine, which is well-documented in (Bettle et al., 2009; Font and García-Peláez, 2013; Font et al., 2010; Watt, 2007). Fig. 5 describes the schematic of the compensation tank blowing during emergency recovery. This process can be divided into three steps. First, the high-pressure air system injects compressed air from the air reservoir into the tank. Therefore, the compensation tank pressure rapidly increases and surpasses the external hydrostatic pressure. Second, the air volume increases inside the compensation tank and expels the bottom of the ballast water. Finally, the buoyancy force becomes larger than the SST weight, forcing the SST to ascent.

Bettle et al. (2009) describe this process as an air-volume ratio in the compensation tank. This mathematic formulation for the SST is represented as:

Table 2
Hydrodynamic derivative.

Parameter	Value	Unit	Parameter	Value	
$X_{\dot{u}}$	-5.14×10^5	kg	$Z_{\|q\|q}$	4.79×10^9	kg•m
$Z_{\dot{w}}$	-3.29×10^7	kg	$M_{\|q\|q}$	-4.34×10^{12}	kg•m^2
$M_{\dot{w}}$	-4.40×10^8	kg•m	X_{wq}	-3.28×10^7	kg
$Z_{\dot{q}}$	-4.40×10^8	kg•m	X_{qq}	-4.40×10^8	kg•m
$M_{\dot{q}}$	-6.39×10^{10}	kg•m^2	Z_{uq}	5.14×10^5	kg
$X_{\|u\|u}$	-1.64×10^4	kg/m	M_{uq}	-4.40×10^8	kg•m
$Z_{\|w\|w}$	-1.42×10^6	kg/m	Z_{uw}	-2.42×10^5	kg/m
$M_{\|w\|w}$	1.67×10^7	kg	M_{uw}	-3.99×10^7	kg

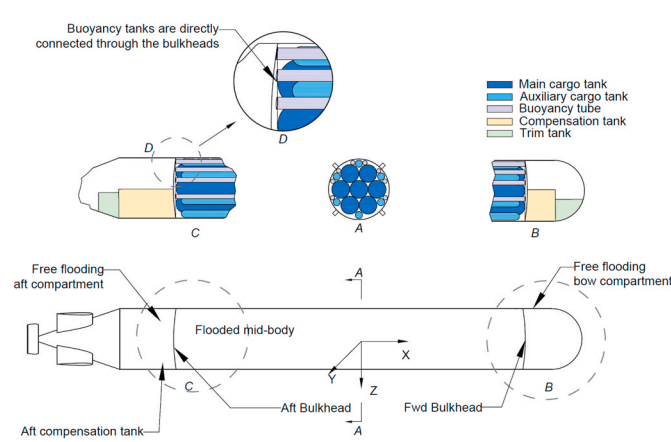

Fig. 4. Subsea Shuttle Tanker tank arrangement (Ma et al., 2021b).

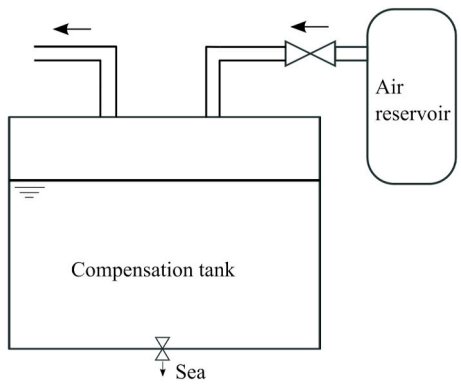

Fig. 5. Schematic of compensation tank blowing.

$$\frac{V_a}{V_t} = A_1 + \sqrt{A_1^2 + A_2^2} \tag{26}$$

$$A_1 = \frac{-p_a - \rho g(z_0 - x_t \sin\theta - 0.45D_t \cos\theta)}{1.8\rho g D_t \cos\theta} \tag{27}$$

$$A_2 = \frac{m_{a0} C_g T(1 - e^{-tC_b})}{0.9\rho g D_t n_t V_t \cos\theta} \tag{28}$$

where V_a is the volume occupied by the air inside the compensation tank, V_t is the volume of a single compensation tank, n_t is the total number of compensation tanks, p_a is the atmospheric pressure, z_0 is the diving depth, x_t is the compensation tank position along the x-axis, D_t is tank diameter, m_{a0} is the initial mass of the compressed air inside the reservoir, C_g is the gas constant, T is the temperature in compensation tanks, t is the time since emergency recovery action is taken, and C_b is the tank blowing constant. The parameters used in compensation tank blowing are listed in Table 3.

2.3. Propeller characteristics

The SST is propelled by a Wageningen B4-70 propeller. The propeller's design parameters are listed in Table 4. Its pitch ratio is 1.0. Its open-water thrust coefficient K_T is adapted from the open-water test result in Smogeli (2006) and interpolated by an 8th-order polynomial function of advance number J. As shown in Fig. 6, the interpolated curve provides a good fit with the test data. The fitted polynomial function is formulated as (29):

$$K_T = -2.157J^8 + 5.006J^7 - 1.399J^6 - 4.309J^5 + 2.999J^4 + 0.564J^3 - 0.998J^2 - 0.133J^2 + 0.444 \tag{29}$$

The advance number J can be calculated by (32):

$$J = \frac{1 - w_T}{nD} u \tag{30}$$

where w_T is the wake fraction, n is propeller rotational speed in revolutions per second, D is the propeller diameter, and u is SST surge velocity.

Table 3
Compensation tank blowing Configuration.

Parameter description	Value	Unit
Compensation tank diameter (D_t)	8	M
Compensation tank x position (x_t)	67.8, −67.8	M
Compensation tank volume (V_t)	800	m^3
Atmospheric pressure (p_a)	1×10^5	Bar
Reservoir air mass (m_{a0})	13,000	kg
Gas constant (C_g)	8.31	$kg{\cdot}m^2{\cdot}s^{-2}{\cdot}K^{-1}{\cdot}mol^{-1}$
Tank temperature (T)	283.15	K
Blowing constant (C_b)	−0.03	–

Table 4
Propeller parameter.

Parameter description	Value	Unit
Selected propeller	Wageningen B4-70	–
Blade number	4	–
Propeller diameter	7	m
Expanded blade ratio	0.70	–
Pitch ratio	1.0	–
Wake fraction	0.47	–
Propeller rotational inertia	4.5×10^5	$kg{\bullet}m^2$
Maximum engine torque	2.5×10^5	N•m

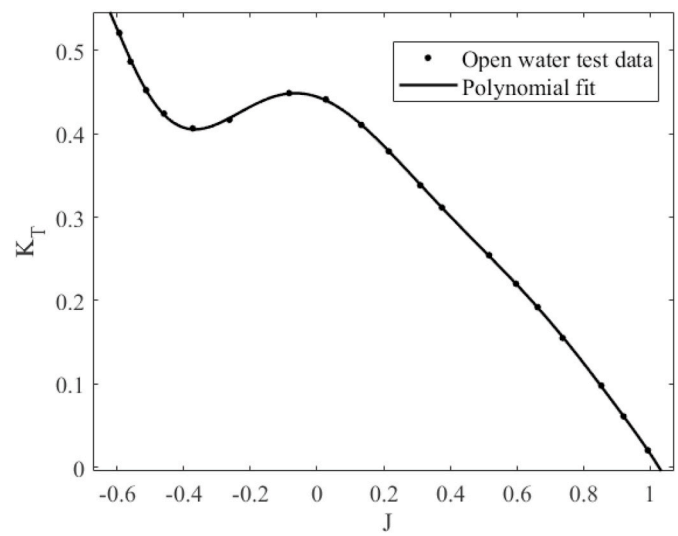

Fig. 6. Propeller thrust coefficient interpolation.

Propeller configurations are presented in Table 4, and a block diagram showing the propeller model is illustrated in Fig. 7. A Proportional–Integral–Derivative (PID) controller is used to control the propeller. The desired propeller rpm and real propeller rpm error goes into the PID controller to calculate the desired motor output. Then, a saturation block represents the maximum limit of motor torque. A second-order transfer function represents rotational inertia from the shaft and propeller. It can simulate response delay caused by motor and shaft dynamics. This usually happens when a rapid change of thrust reference occurs. Finally, the propeller's real-time thrust is calculated by propeller revolution speed and SST surge velocity.

2.4. Control plane

The control planes' contribution to the forces and moment on the SST is modelled using a linear lift rate coefficient. The control forces generated by a single control plane can be calculated as:

$$X_{\delta c} = -0.5\rho V^2 A_c C_{D\delta} \tag{31}$$

$$Z_{\delta c} = 0.5\rho V^2 A_c C_{L\delta} \tag{32}$$

$$M_{\delta c} = 0.5\rho V^2 A_c x_c C_{L\delta} \tag{33}$$

where $X_{\delta c}$ is control plane drag, $Z_{\delta c}$ is control plane lift, $M_{\delta bow}$ is the control plane pitch moment. V is the relative velocity at the plane position, $C_{D\delta}$ is the drag rate coefficient, $C_{L\delta}$ is the lift rate coefficient. The bow and aft control plane configurations are listed in Table 5.

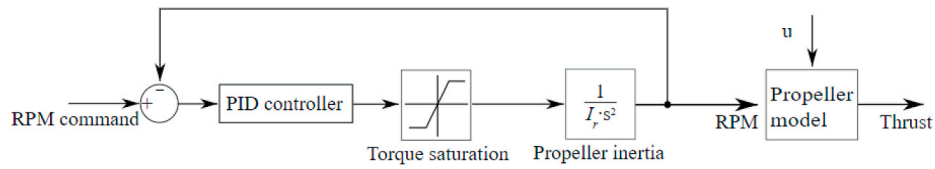

Fig. 7. Propeller diagram.

Table 5
Control plane parameter.

Parameter description	Value	Unit
Bow plane position (x_{bow})	30	m
Bow plane area (A_{bow})	50	m^2
Bow plane lift rate coefficient ($C_{L\delta}$)	2.1	–
Bow plane angle rate limit	±5	°/s
Aft plane position (x_{aft})	−70	m
Aft plane area (A_{stern})	28	m^2
Aft plane lift rate coefficient ($C_{L\Delta\delta}$)	6.1	–
Aft plane angle rate limit	±5	°/s

3. Accidental case and standard operation procedure

An SOE is generated by running a wide range of simulations according to different accidents (Park and Kim, 2018; Renilson, 2018). Hence, it is essential to define the SOP when each failure happens. When a failure occurs, the SST should react following a set of SOPs. In this section, SOPs with regard to accidental cases are defined. The criterion of successful recoveries and lost-of-vessel are identified.

3.1. Partial flooding

Renilson (2018) defines the flooding of a submarine happens through the systems connected to the sea, which are typically kept closed. This may happen to the valves for loading and offloading or loading ballast for the SST. Flooding is risky when the SST is travelling at a slow speed.

Fig. 8 presents the SST flounder diagram. It is a length versus cross-section diagram that describes the volume distribution of the vessel without showing a detailed layout. Flooding can occur in the free flooding compartments, i.e., the machinery compartments. In this study, an unclosed valve at the aft compartment is considered. When flooding happens in the aft compartment, three actions are taken to perform emergency recovery. The first action is to apply full forward rpm to increase the speed. Second, the main ballast tanks will be blown to increase the buoyancy of the SST. Third, maximum bow plane angle is executed to generate lift force forcing SST to ascent. From experience taught by naval submarines, an unpowered and high-rate rising manoeuvre may cause instability in the horizontal plane and induce considerable roll motion (Bettle et al., 2009; Chen et al., 2020; Watt, 2001, 2007; Zhang et al., 2019). To avoid this effect, Renilson (2018) suggested that the pitch angle should be limited during emergency rising, and blow should be performed in all ballast tanks together rather than in the forward ballast tank only to remain stable. When flooding

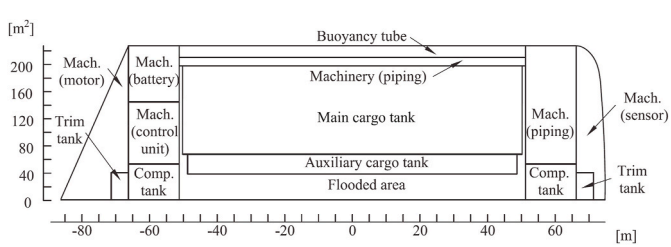

Fig. 8. SST flounder diagram (Ma et al., 2021b).

happens, the SST is recovered if it reaches the sea surface without exceeding the maximum trimming angle, exceeding the maximum diving depth, or reaching the seabed.

The flooding rate is modelled as:

$$r = \rho A_{fld}\sqrt{2gh_d(t)} \tag{34}$$

where r is the seawater flood rate with a unit of kg/s, $A_{fld} = 0.785\ m^2$ is the area of the opening, and $h_d(t)$ is SST diving depth at time t. During the simulations, the maximum flooded volume is 600 m^3, as the free flooding area is also divided into small compartments by watertight bulkheads.

3.2. Control plane jamming

SST uses an independently actuated X-plane arrangement. Therefore, a single control plane jam is considered a failure mode, and the rest three planes can still be used for roll control. The control plane jamming failure of the SST can lead to two consequences: jam-to-rise or jam-to-dive. The SST should conduct different procedures for each case. The emergency recovery action to cope with the control plane jamming failure is given as below:

3.2.1. Jam-to-rise

A crash stop manoeuvre is performed when the jam-to-rise failure occurs. The SST takes two actions simultaneously: it orders a full astern RPM to reduce its forward velocity and executes a maximum positive bow plane angle to stop the ascent. Like jam-to-dive recovery action, the three free aft control planes hold the heel angle. In a jam-to-rise situation, the SST survives if it does not broach the surface or reach the pitch limit.

3.2.2. Jam-to-dive

When the SST suffers from a jam-to-dive situation, the recovery is divided into two actions: the first action is a crash stop manoeuvre, and an order of full rpm astern is conducted. As for the second action, the SST pumps out its ballast in the forward compensation tank and executes the most negative bow control plane angle. These actions provide a positive buoyancy force and reduce its trimming angle. The SST survives if SST achieves a trajectory upwards before hitting the seabed or exceeds the collapse depth. However, the maximum trimming angle should not be exceeded either.

3.3. Manoeuvring limits

A set of manoeuvring limits are defined when setting up the SOE. These limits include depth limits, pitch angle limits, control plane reaction angles, and SST reaction time. The manoeuvring limits for setting up the SOE are listed in Table 6. The most critical definitions are given as follows:

- Safety depth: the safety depth is the minimum operational depth of the SST. If the SST travels above this depth, it risks collision with large draught ships and other offshore structures. DNV naval submarine code recommends submarines to travel below 30–40 m water depth (DNV, 2018).

Table 6
SST manoeuvring limitations.

Parameter description	Value	Unit
Safety depth	40	m
Nominal diving depth	70	m
Collapse diving depth	190	m
Pitch angle restriction	10,15,20	°
Aft control plane jam angle	15	°
Bow control plane reaction angle	20	°
Reaction time	0	s

- Nominal diving depth: the SST is allowed to perform unrestricted operation above this depth but below the safety depth. This value is defined to be 70 m for the SST.
- Collapse diving depth: the hydrostatic pressure at collapse diving depth is the 19-bar designed pressure for the SST. Therefore, the collapse diving depth is decisive for the structural design of the SST.
- Pitch angle restriction: because the SST is autonomous, the maximum pitch angle is not restricted by the human factor, i.e., the safety of crew members. However, an overlarge pitch inclination may also induce malfunction of machinery and equipment onboard. Meanwhile, a large pitch angle is dangerous during high-speed operation: the SST transits from nominal diving depth to the collapse diving depth within a minute. This leaves insufficient time for the recovery action when the control plane jam happens. In practice, Burcher (Burcher and Rydill, 1994) suggested that the maximum pitch angle of submarines is around 20°. In the event of a high-speed operation, the pitch limit is 5–10°. Emergency recoveries at 10°, 15°, and 20° initial pitch angles are performed in this work
- Reaction time: the reaction time is defined as the time interval between the malfunction and recovery action. The high level of autonomy can significantly reduce the reaction time from seconds to milliseconds. Therefore, the SST provides an instant reaction when failure happens.

4. Results and discussion

This paper discusses the generation of the safety operational envelope of a baseline SST. Three malfunctions, i.e., flooding, aft control plane jam-to-rise, and aft control plane jam-to-dive, are considered individually during the study. 37 free-running tests with three initial pitch angles and 14 different initial speeds are performed by the authors in Simulink. Each simulation lasts 1000 s to dampen out the initial transient period and reach steady-state conditions. Also, this simulation time is long enough to capture each simulation's maximum and minimum depth excursion. Later, the time interval between the incident and emergency recovery action succeed is selected in the post-processing stage. In this section, three simulation results are discussed in detail to present the SST behaviour during emergency recovery when aft compartment flooding, jam-to-rise, and jam-to-dive happen. Then, the manoeuvring limitations of SST are presented at a wide range of depths, pitch angles, and velocities. Finally, the desired depth and speed range are determined, and the SOE in this range is presented.

4.1. Aft compartment flooding recovery response

Fig. 9 presents the depth excursion and pitch motion of the SST after flooding occurs. In this case, the initial speed of the SST is 0 m/s, i.e., the flooding happens right after the SST offloads at a subsea well. The SST hovers at 114 m water depth during offloading. In the presented time series, the flooding incident starts from t = 50 s. After the incident occurs, the SST immediately executes recovery action following the SOP. The entire process takes approximately 150 s. In the first 50 s, the descent of SST speeds up. Later after t = 100 s, the recovery action effects show up as the descent speed decreases. At t = 205 s, the maximum 190 m depth is reached. The descent speed reduces to 0. After this time, the SST floats up and avoids the lost-of-vessel. As for the pitch, since flooding happens at the SST aft, the weight at the aft increases. This introduces a negative pitch moment. The pitch angle rapidly increases in the beginning after the incident happens. This trend becomes mild afterwards due to the increase of the hydrostatic restoring moment.

Fig. 9 (b) presents the surge and heave velocities in the aft compartment flooding process. They are measured in the body-fixed reference frame. In the initial 50 s, both surge and heave velocity are 0 m/s. As shown in Fig. 9 (c), a 60-rpm propeller command is ordered when the incident happens. A PID controller controls the propeller. As the SST has a large inertia, there is a 10 s delay in the surge velocity. The propeller thrust provides the most critical contribution during the recovery process. It pushes the SST upward when the pitch angle is negative. Besides, the SST slides downward in the body coordinate throughout the process, i.e., the heave velocity is always positive. This is because the weight of the SST is always larger than the displacement after flooding happens. The heave velocity reduces after approximately 90 s because of the blowing of the compensation tank and the increasing upward hydrodynamic body drag introduced by the relative velocity between SST and the incoming flow.

Fig. 9 (d) shows the process of flooding and blowing the compensation tank. Due to the 11.4 bar hydrostatic pressure, a 600 m^3 compartment is filled with seawater within 20 s. As for the performance of tank blowing, both the tank blowing rate and maximum blowing volume depend on the hydrostatic pressure. At a depth of 190 m, a single compensation tank can blow 258 m^3, i.e., 265 tonnes of seawater. When this is counted into net buoyancy, a −4000 kN minimum net buoyancy is reached when t = 70 s. After that, the net buoyancy increases to −841 kN at 205 s. This indicates that although performing tank blowing alone cannot overcome flooding at a greater water depth; it can still help to moderate the descent speed.

4.2. Jam-to-rise recovery response

Fig. 10 presents the response of the SST under a jam-to-rise incident when the initial speed and pitch angle are 3 m/s and −15°, respectively. Fig. 10 (a) shows the heave and pitch motions of the SST. The recovery actions include the application of the emergency brake of the propeller and the command to go to maximum bow control plane angle. Before the aft control plane jams, the SST rises upward at a −15° pitch angle. When recovering from a jam-to-rise incident, the SST survives if it stops its ascent before broaching the surface, i.e., it cannot rise more than 40 m. The entire process takes around 170 s in this incident. In the presented case, the incident happens at t = 55 s and the SST stops ascent at t = 225 s. The minimum depth excursion is −38.5 m, 1.5 m below the surface. The pitch angle of the SST slowly increases from −15° to −4° in this period. Fig. 10 (b) shows the surge and heave velocity of the SST in the body-fixed reference frame. The surge velocity drops from 3 m/s to 2.2 m/s in the presented time series. The heave velocity in the body frame is positive throughout the process. Fig. 10 (c) shows the propeller revolution, bow control plane angle, and aft control plane angle of the SST during the recovery. A slow propeller response is observed due to the large rotational inertia. The propeller rpm reduces from 30 rpm to 0 rpm within 17 s for the first time and overshoots to −7 rpm. It reaches the ordered revolution speed at t = 135 s. As for the plane angles, the aft control planes are jammed at 15°, and the bow control plane angle changes from 0 to 20° during the recovery process. This generates a positive fin lift to reduce the rising of the SST.

4.3. Jam-to-dive recovery response

An example of jam-to-dive recovery at 5 m/s initial speed is given in this section. The jam-to-dive happens at t = 50 s. The entire recovery process takes approximately 100 s. The initial pitch angle is set to be 15° when the incident occurs. Fig. 11 (a) presents the maximum depth excursion and the pitch angle of the SST during the recovery process.

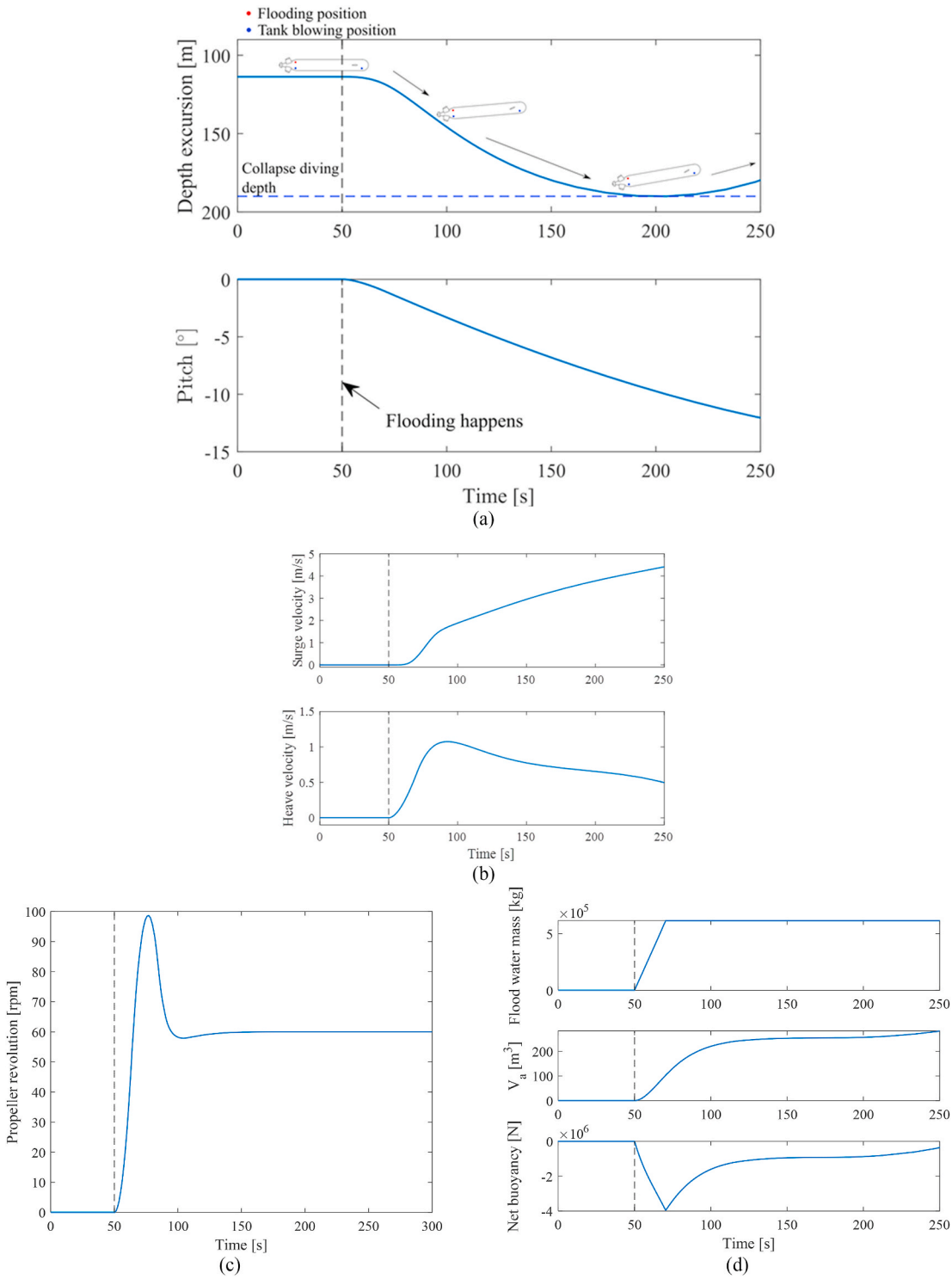

Fig. 9. SST responses during emergency recovery from flooding.

The maximum recoverable depth is found to be 100 m. The SST stops descending at 190 m water depth beginning from this depth. As for SST pitch angle, it changes from 15° to 6° in 100 s. This is faster than the jam-to-rise incident because of the blowing of the forward compensation tank. The surge and heave velocities in the body-fixed reference frame are presented in Fig. 11 (b). As the inertia of the SST is large, it takes time for the surge speed to reduce to 0. The heave velocity decreases rapidly after the forward compensation tank blowing is performed and becomes negative at t = 110 s.

However, in the NED frame, the SST stops diving 40 s later. Fig. 11 (c) shows the response from propeller and control planes. At t = 50 s, a 0-rpm command is ordered. First, the propeller rapidly reduces its rotational speed and reaches an astern revolution speed of −25 rpm. Then, it increases to 0 rpm around t = 100 s. As for the bow control plane, a minimum −20° angle is executed when the SST is released at t = 50 s. The aft control plane is jammed at a −15° maximum angle during the process. The forward compensation tank blowing process is presented in Fig. 11 (d). The blow rate (curve slope in Fig. 11 (d)) first reduces with the increasing SST diving depth due to the greater hydrostatic pressure. Then it increases again when the SST starts to ascent.

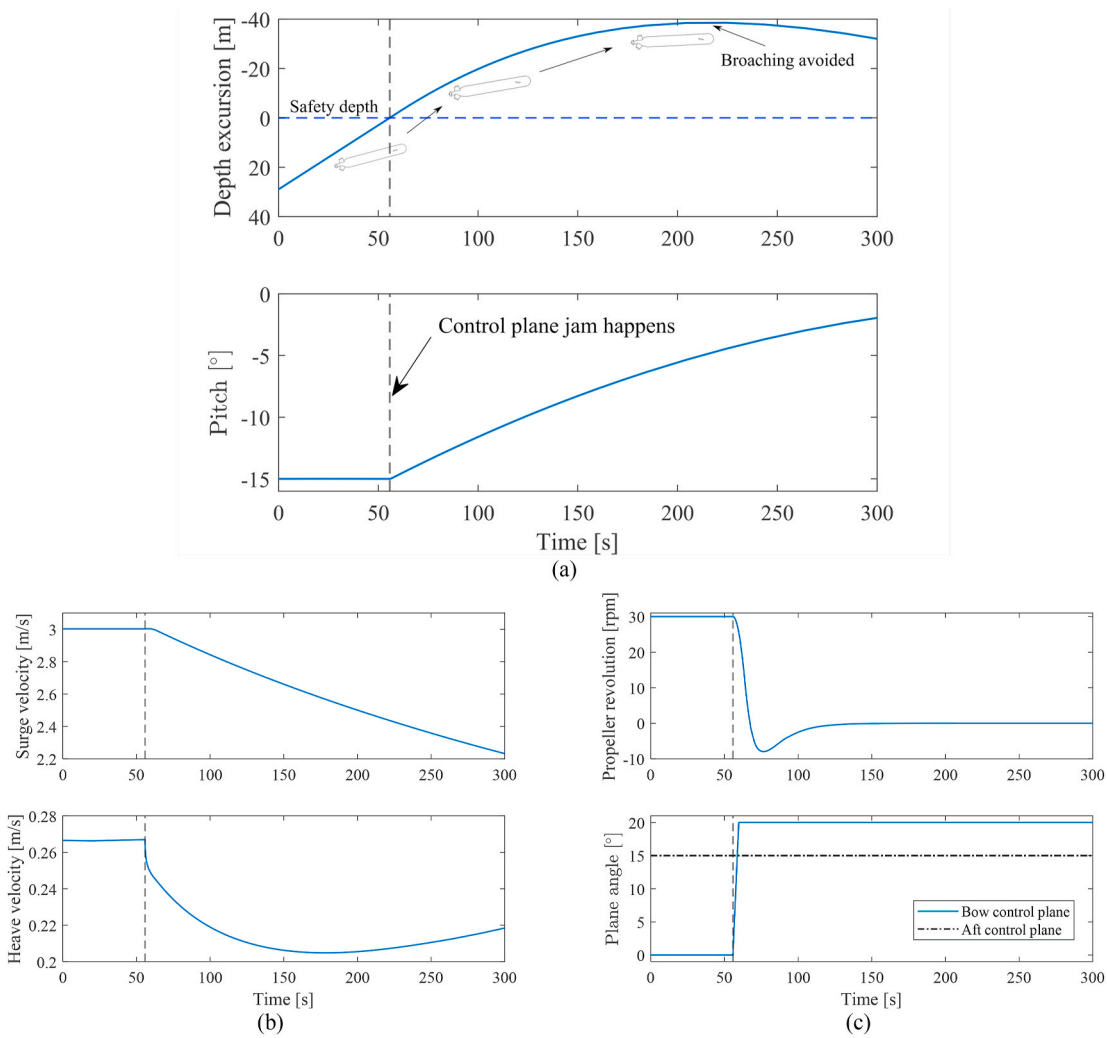

Fig. 10. SST responses during emergency recovery from jam-to-rise at 3 m/s service speed.

4.4. Operation limitations

Results of the 37 simulated cases are presented in Fig. 12. From a safety manoeuvring perspective during the operation, the SST is not suggested to sail above the jam-to-rise lines, below the flooding line, or below the jam-to-dive lines.

Aft compartment flooding: The SST must operate above the flooding limit line (shown in Fig. 12 (a)) to be recoverable from aft compartment flooding. It is most detrimental when the SST travels slowly as insufficient lift forces are generated from the SST body and control planes. As shown in Fig. 12 (a), the maximum recoverable depth is 80 m when the SST hovers (0 forward speed). This value rises to 110 m at 3 m/s design speed. Both of these depths are greater than the 70-m nominal diving depth of the baseline SST. This indicates that the SST is recoverable from an aft compartment flooding event when travelling below the nominal diving depth.

Jam-to-rise: The SST must operate below the jam-to-rise lines to avoid broaching the surface when the control plane jams. The initial pitch angles are set to 10°, 15°, and 20° when jam-to-rise happens. The results are shown as the solid lines in Fig. 12. As the SST is designed to travel slowly to reduce energy consumption, the region between 0 m/s to 6 m/s is of the most interest. The $\theta = 10°$ limit does not affect the result in this speed region. When the SST travels faster than 3 m/s, its pitch angle limit is 15°. If the SST travels below this speed, a 20° restriction is applied to avoid structural and machinery damage instead of control plane jam.

Jam-to-dive: The SST must operate above the jam-to-dive lines to avoid exceeding the collapse diving depth when the control plane jams. Same with the jam-to-rise scenario, the $\theta = 10°$ limit does not affect the result as the speed region will never be reached (above 8 m/s). In addition, the $\theta = 20°$ limitation does not affect the depth limit either, as the $\theta = 20°$ jam-to-dive line (dashed, circle) located below the flooding limit (dash-dotted, asterisk) in Fig. 12. Therefore, $\theta = 15°$ limit has the most considerable effect on the SST operation. In addition, the SST is recoverable from a jam-to-rise when travelling slower than 5 m/s at a water depth above 100 m. This indicates that the 70 m nominal operational depth is conservative when considering the recoverability in a jam-to-dive situation.

Based on the designed operating velocities and depth limits mentioned above, an envelope is drawn in Fig. 12 (b). This gives the basis for the SOE presented in Fig. 13. The figure envelopes the depth range from 0 m to 190 m, and the velocity range from 0 m/s to 6 m/s. This can cover all possible operating conditions of SST under regular situations. In the envelope, the broaching avoid zone is set between 0 m and 40 m safety depth. The SST is allowed to travel below 40 m water depth at a maximum speed of 3 m/s. Above this speed, the SST has to travel at a greater depth to avoid an unrecoverable jam-to-rise incident. The operational zone is divided into unrestricted and restricted areas. The SST can recover from the considered malfunctions during all kinds of manoeuvres in the former area. In the restricted operation area, a 15° maximum pitch angle restriction is posed on the SST to avoid an unrecoverable control plane jam incident. In addition, the 70 m nominal

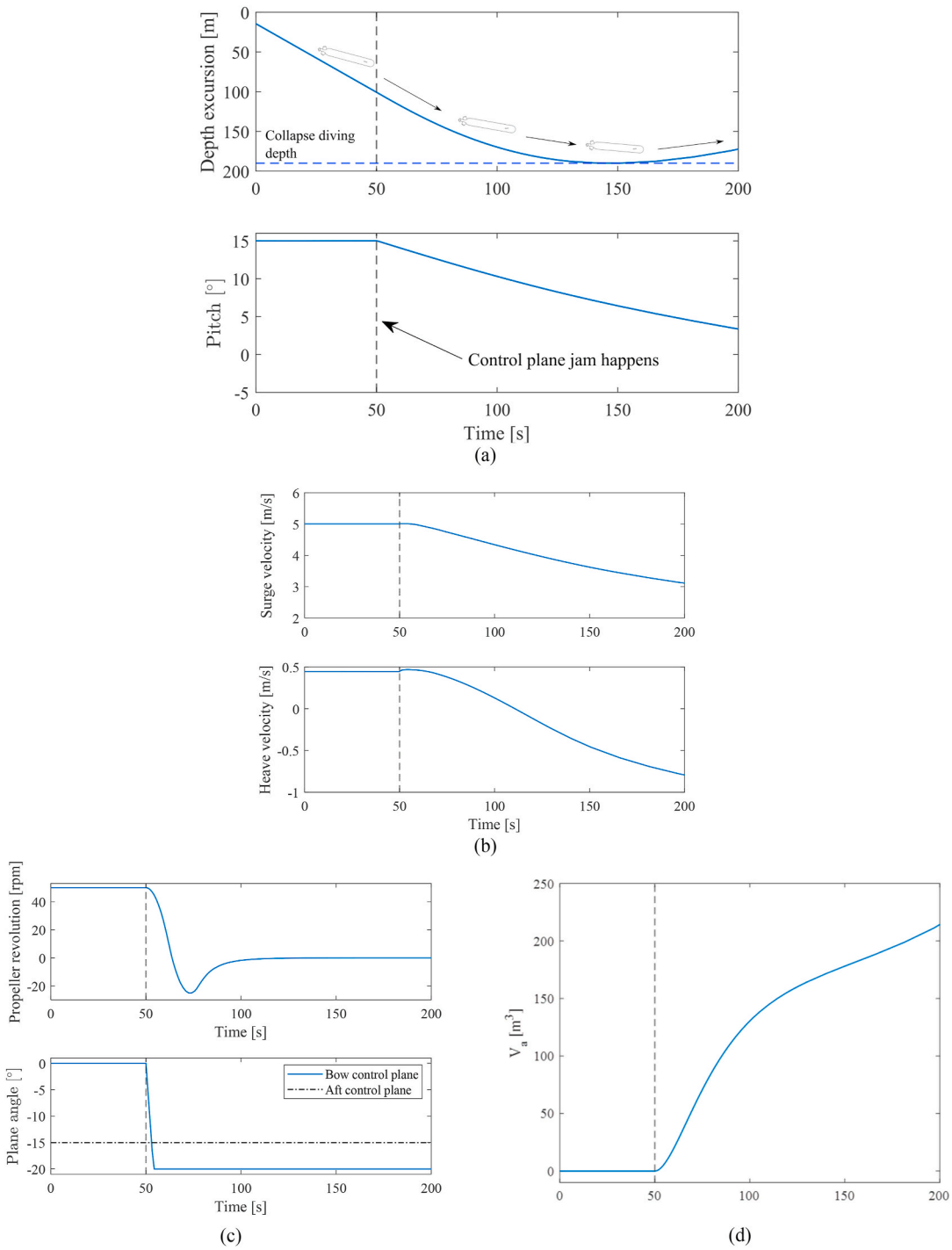

Fig. 11. SST responses during emergency recovery from jam-to-dive at 5 m/s initial speed.

diving depth is conservative from the manoeuvring perspective. When the baseline SST travels at 3 m/s speed, a 100 m operational depth is proposed. This allows the SST to recover from a partial flooding incident or a jam-to-dive incident when travelling between 2 m/s to 5 m/s speed, i.e., 67%–167% of the designed speed. This is enough to cover the normal operation of the SST, which constantly travels at a fixed speed. Moreover, it can also be noticed that flooding is the main concern when the SST operates at a slow speed (less than 2 m/s), while control plane jam is riskier when the SST speed is above 3 m/s.

5. Conclusions

A baseline SST was proposed as an innovative alternative to tanker ships and subsea pipelines. This paper presents the identification of the SOE of the SST. The SOE is a crucial topic in the SST design process as it demonstrates the recoverability of the SST under critical malfunctions, including partial flooding, jam-to-rise, and jam-to-dive. Even though SOE has been established for military submarines for over 50 years, public literature on such analyses is still not readily available. In addition, as very few submarines have been designed for civilian use, this paper will also help close this knowledge gap and further assist the development and safety operation of large novel subsea vessels. This is

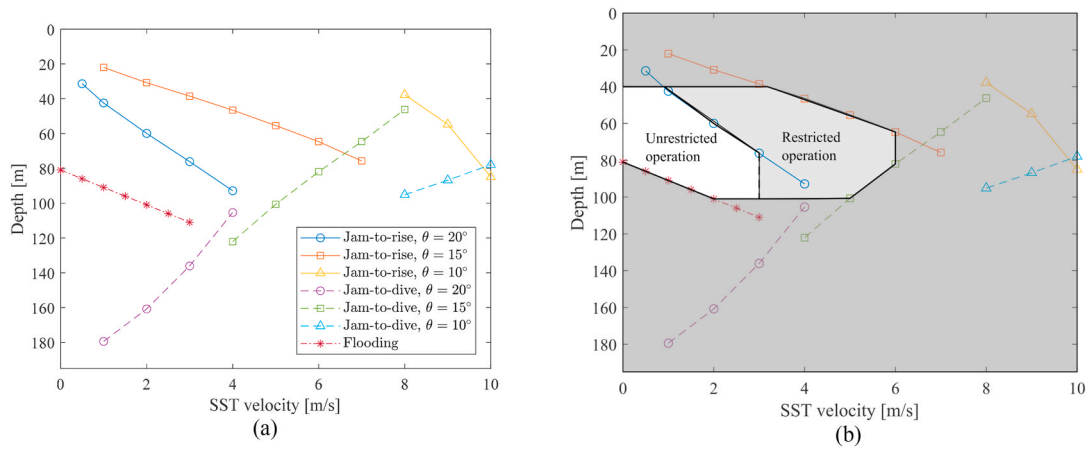

Fig. 12. Operation limitations (a) and the SOE (b) of the SST.

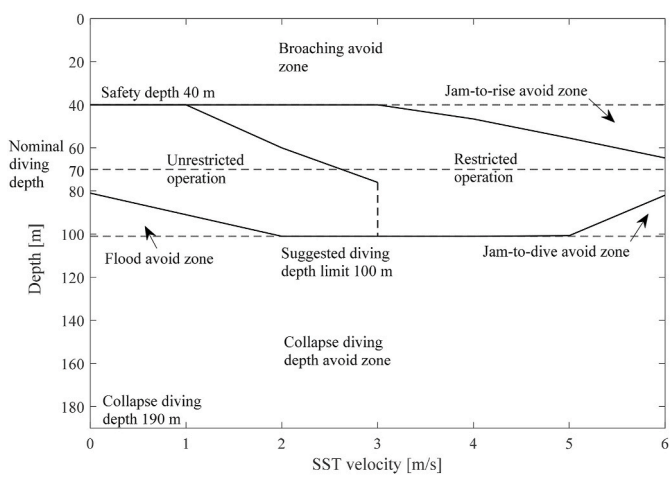

Fig. 13. Final SST safety operational envelope.

especially so as most submarine manoeuvring software is developed for military submarines.

One limitation of the study is that the SST manoeuvring model is developed based on semi-empirical formulas. This is generally sufficient for the SST, which is at a conceptual design stage. However, for detailed engineering designs with a much higher required level of accuracy, the model must be updated with more accurate hydrodynamic derivatives obtained from computational fluid dynamic analyses or model tests. However, it is also highlighted that civilian submarines will be larger and restricted in their manoeuvrability. Therefore, the effect of nonlinearity in the derivatives-based hydrodynamic models is less pronounced. This means the proposed model can better describe SST than naval submarine motions.

The authors first derived a manoeuvring simulation model following semi-empirical formulas in the paper. This model considers combined load effects from hydrodynamic loads, compensation tank blowing, propeller thrust, and control plane lift. Second, standard operation procedures are defined individually for flooding, jam-to-rise, and jam-to-dive. Third, SST dynamic responses during the recovery actions are discussed. Fourth, operation limitations considering different initial depths, sailing speeds, and pitch angle combinations are presented. Finally, the SOE of the SST is presented based on the obtained result.

The SOE helps to improve the currently existing design and operation of the SST in the following aspects:

- A 40 m safety depth is sufficient to allow the SST to avoid broaching the surface when the aft control plane jams when travelling at 3 m/s design speed. If a higher sailing speed is required, the SST has to travel at deeper water depths.
- The SST can survive all considered malfunctions when travelling at a 70 m nominal water depth.
- The SST should hover above 80 m water depth during offloading to recover from partial flooding.
- The maximum pitch angle of the SST is set to be ±15°. Within this limit, the SST is recoverable if the aft control plane jam occurs.
- The 70 m nominal diving depth proposed by the DNV naval submarine code is conservative. The SOE allows the existing SST design to travel a maximum 100 m diving depth in accordance with a 190 m collapse diving depth. This depth can fulfil operation safety as the SST can survive the considered crucial malfunctions.
- Otherwise, the safety factor between nominal and collapse diving depths can be reduced. This can reduce SST structural weight and avoid heavy and complex steel construction.

CRediT authorship contribution statement

Yucong Ma: Conceptualization, Methodology, Formal analysis, Software, Data curation, Writing – original draft. **Yihan Xing:** Conceptualization, Methodology, Supervision, Writing – review & editing, Project administration.

Declaration of competing interest

The authors declare that they have no known competing financial interests or personal relationships that could have appeared to influence the work reported in this paper.

Data availability

Data will be made available on request.

Acknowledgement

The authors declare that they have no known competing financial interests or personal relationships that could have appeared to influence the work reported in this paper.

References

Bettle, M.C., Gerber, A.G., Watt, G.D., 2009. Unsteady analysis of the six DOF motion of a buoyantly rising submarine. Computers & Fluids 38 (9), 1833–1849. https://doi.org/10.1016/j.compfluid.2009.04.003.

Blevins, R.D., 1979. Formulas for Natural Frequency and Mode Shape. Van Nostrand Reinhold Co., New York.

Burcher, R., Rydill, L., 1994. Concepts in Submarine Design. Cambridge University Press, Cambridge.
Chen, Q., Li, H., Zhang, S., Wang, J., Pang, Y., Wang, Q., 2020. Effect of waves on the behavior of emergent buoyantly rising submarines using CFD. Applied Sciences 10 (23), 8403. https://doi.org/10.3390/app10238403.
DNV, 2018. Rules for Classification, Naval Vessels, Part 4 Sub-surface Ships (Chapter 1) Submarines.
Ellingsen, K.E., Ravndal, O., Reinås, L., Hansen, J.H., Marra, F., Myhre, E., Dupuy, P.M., Sveberg, K., 2020. RD 677082-Subsea Shuttle System. Research Disclosure.
Equinor Energy AS, 2019. RD 662093-Subsea Shuttle System. Research Disclosure.
Faltinsen, O., 1993. Sea Loads on Ships and Offshore Structures. Cambridge University Press, Cambridge.
Font, R., García-Peláez, J., 2013. On a submarine hovering system based on blowing and venting of ballast tanks. Ocean Engineering 72, 441–447. https://doi.org/10.1016/j.oceaneng.2013.07.021.
Font, R., García, J., Ovalle, D., 2010. Modelling and Simulating Ballast Tank Blowing and Venting Operations in Manned Submarines, 8th IFAC Conference on Control Applications in Marine Systems. Rostock-Warnemude, Germany. https://doi.org/10.3182/20100915-3-de-3008.00029.
Fossen, T.I., 2011. Handbook of Marine Craft Hydrodynamics and Motion Control. John Willey & Sons, Ltd, West Sussex, UK.
Giddings, A.J., Louis, W.L., 1966. Overcoming submarine control-surface jams and flooding casualties. Navel Engineerings Journal 78 (6), 1055–1067. https://doi.org/10.1111/j.1559-3584.1966.tb04132.x.
Hoerner, S.F., 1965. Fluid-dynamic Drag: Practical Information on Aerodynamic Drag and Hydrodynamic Resistance. Published by the author, California, USA.
Jacobsen, L., Lawrence, K., Hall, K., Canning, P., Gardner, E., 1983. Transportation of LNG from the arctic by commercial submarine. Marine Technology and SNAME News 20 (4), 377–384. https://doi.org/10.5957/mt1.1983.20.4.377.
Jacobsen, L.R., 1971. Subsea Transport of Arctic Oil - a Technical and Economic Evaluation. Offshore Technology Conference, Houston, Texas. https://doi.org/10.4043/1425-MS.
Jacobsen, L.R., Murphy, J.J., 1983. Submarine transportation of hydrocarbons from the arctic. Cold Regions Science and Technology 7, 273–283. https://doi.org/10.1016/0165-232X(83)90073-3.
Kery, S.M., Eaton, M., Henry, S.C., Vasilakos, J., Kery, S.M., 2018. On the Creation of a Safe Operating Envelope for Ships. SNAME Maritime Convention, Rhode Island, USA.
Lombaerts, T.J.J., Schuet, S.R., Wheeler, K.R., Acosta, D., Kaneshige, J.T., 2013. Safe maneuvering envelope estimation based on a physical approach. In: AIAA Guidance, Navigation, and Control Conference 2013, Boston, MA.
Ma, Y., Sui, D., Xing, Y., Ong, M.C., Hemmingsen, T.H., 2020. Depth control modelling and analysis of a subsea shuttle tanker ASME 2021 40th international conference on ocean, offshore and arctic engineering. Virtual. https://doi.org/10.1115/OMAE2021-61827. Online.
Ma, Y., Xing, Y., Hemmingsen, T., 2021a. An Evaluation of Key Challenges of CO_2 Transportation with a Novel Subsea Shuttle Tanker, COTech & OGTech 2021. IOP Publishing, Stavanger, Norway. https://doi.org/10.1088/1757-899X/1201/1/012078.
Ma, Y., Xing, Y., Ong, M.C., Hemmingsen, T.H., 2021b. Baseline design of a subsea shuttle tanker system for liquid carbon dioxide transportation. Ocean Engineering 240. https://doi.org/10.1016/j.oceaneng.2021.109891.
Ma, Y., Xing, Y., Sui, D., 2022. Trajectory envelope of a subsea shuttle tanker hovering in stochastic ocean current - model development and tuning. Journal of Offshore Mechanics and Arctic Engineering. https://doi.org/10.1115/1.4055282.
Marchant, P., Kimber, N., 2014. Assuring the Safe Operation of Submarines with Operator Guidline. Underwater Defence Technology, Liverpool, UK.
MathWorks, 2022. Simulink User's Guide. The MathWorks, Inc., MA, USA.
Moloney, M.P., 1974. Submarine Tanker Concepts and Problems. National Maritime Research Center.
Park, J.-Y., Kim, N., 2017. Design of a safety operational envelope protection system for the pitch angle of a submarine. Proceedings of the Institution of Mechanical Engineers, Part M: Journal of Engineering for the Maritime Environment 231 (2), 441–451. https://doi.org/10.1177/1475090216644281.
Park, J.-Y., Kim, N., 2018. Design of a safety operational envelope protection system for a submarine. Ocean Engineering 148, 602–611. https://doi.org/10.1016/j.oceaneng.2017.11.016.
Prestero, T., 2001. Verification of a Six-Degree of Freedom Simulation Model for the REMUS Autonomous Underwater Vehicle. Massachusetts Institute of Technology & Woods Hole Oceanographic Institution. https://doi.org/10.1575/1912/3040.
QinetiQ, 2018. The Influence of Aft Control Surface Configuration of a Submarine on the Submerged Operational Performance. Underwater Defence Technology, Glasgow.
Renilson, M., 2018. Submarine Hydrodynamics. Springer International Publishing AG, Cham, Switzerland.
Ross, A., Fossen, T.I., Johansen, T.A., 2004. Identification of underwater vehicle hydrodynamic coefficients using free decay tests. In: IFAC Conference on Computer Applications in Marine Systems. Elsevier BV, Ancona, Italy, pp. 363–368. https://doi.org/10.1016/s1474-6670(17)31759-7.
Schjølberg, I., Utne, I.B., 2015. Towards Autonomy in ROV Operations, 4th IFAC Workshop onNavigation, Guidance and Controlof Underwater VehiclesNGCUV 2015, Girona, Spain. https://doi.org/10.1016/j.ifacol.2015.06.030.
Smogeli, Ø.N., 2006. Control of Marine Propellers-From Normal to Extreme Conditions. Department of Marine Technology. Norwegian University of Science and Technology, Trondheim.
Taylor, P.K., Montgomery, J.B., 1977. Arctic Submarine Tanker System Offshore Technology Conference, Houston, Texas. https://doi.org/10.4043/2998-MS.
Tingle, C., 2009. Submarine accidents a 60-year statistical assessment. Professional Safety 54 (9).
Tinker, S.J., 1982. Identification of submarine dynamics from free-model test. In: Admiralty Marine Technology Establishment, UK, Proceedings of the DRG Seminar on Advanced Hydrodynamic Testing Facilities, Session 3, Paper 16, The Netherlands. Paper: P1982-1.
Watt, G.D., 2001. A Quasi-Steady Evaluation of Submarine Rising Stability: the Stability Limit, NATO Research and Technology Organisation Applied Vehicle Technology Panel Symposium, Leon, Norway.
Watt, G.D., 2007. Modelling and Simulating Unsteady Six Degrees-Of-Freedom Submarine Rising Maneuvers. Defence Research and Development Canada-Atlantic. Canada, Dartmouth.
Xing, Y., 2021. A conceptual large autonomous subsea freight-glider for liquid CO2 transportation. In: ASME 2021 40th International Conference on Ocean, Offshore and Arctic Engineering, Virtual. https://doi.org/10.1115/omae2021-61924. Online.
Xing, Y., Ong, M.C., Hemmingsen, T., Ellingsen, K.E., Reinås, L., 2021a. Design considerations of a subsea shuttle tanker system for liquid carbon dioxide transportation. Journal of Offshore Mechanics and Arctic Engineering 143 (4). https://doi.org/10.1115/1.4048926.
Xing, Y., Santoso, T.A.D., Ma, Y., 2021b. Technical-economic feasibility analysis of subsea shuttle tanker. Journal of Marine Science and Engineering 10 (1), 20. https://doi.org/10.3390/jmse10010020.
Zhang, S., Li, H., Zhang, T., Pang, Y., Chen, Q., 2019. Numerical simulation study on the effects of course keeping on the roll stability of submarine emergency rising. Applied Sciences 9 (16), 3285. https://doi.org/10.3390/app9163285.